MATERIALS CHEMISTRY
FRONTIERS

RESEARCH ARTICLE

View Article Online
View Journal | View Issue

Cite this: *Mater. Chem. Front.*, 2023, **7**, 1128

Efficient narrowband green OLEDs with TADF sensitizers combining multiple charge-transfer pathways†

Deli Li, Jiaji Yang, Jiting Chen, Xiaomei Peng, Wei Li, Zijian Chen, Weidong Qiu, Guo-Xi Yang, Zhihai Yang, Mengke Li, Simin Jiang, Denghui Liu, Yiyang Gan, Kunkun Liu and Shi-Jian Su *

Received 28th December 2022,
Accepted 31st January 2023

DOI: 10.1039/d2qm01363k

rsc.li/frontiers-materials

Multiple resonance (MR) thermally activated delayed fluorescence (TADF) emitters have attracted much attention for their narrow emission band and high efficiency. However, organic light-emitting devices based on MR-TADF emitters generally suffer from severe efficiency roll-off at high current density due to their relatively large singlet–triplet splitting energy. In this work, three TADF molecules are designed by an *ortho*-connected oligo carbazole donor and diphenyltriazine acceptor with the purpose of combining both through-bond charge transfer (TBCT) and through-space charge transfer (TSCT). Through fine tuning the proportion of intramolecular TBCT and TSCT by changing the number of carbazole units, a relatively high reverse intersystem crossing rate (k_{RISC}) approaching 10^6 s^{-1} and radiative transition rate (k_F) of over 10^6 s^{-1} are achieved. As a result, the devices using these molecules as emitters give maximum external quantum efficiency (EQE) of over 20% with extremely low efficiency roll-off of 9.9% at the practical luminance of 1000 cd m^{-2}. Furthermore, by using these materials as assistant hosts and sensitizers and DMAc-BN as a terminal emitter, high efficiencies of 23.9% and 66.0 lm W^{-1} are achieved with a full width at half maximum of 46 nm, featuring slow efficiency roll-off with EQE of 17.9% at the luminance of 1000 cd m^{-2}.

Introduction

Thermally activated delayed fluorescence (TADF) materials have attracted global attention from the academic and industrial communities since the pioneering work of the purely organic TADF organic light-emitting diodes (OLEDs) developed by Adachi and coworkers.[1–3] Owing to the unity exciton utilization comparable to noble-metal-containing phosphorescence materials and much higher than traditional fluorescence materials, as well as facile property modulation through manipulating the charge transfer (CT) characteristics, TADF materials hold great potential to achieve high performance OLEDs.[4–6] Through-bond charge transfer (TBCT) and through-space charge transfer (TSCT) are two general CT characteristics for developing TADF materials.[4,6–9] High radiative transition rate (k_F) and reverse intersystem crossing (RISC) rate (k_{RISC}) are indispensable for TADF materials to achieve high external quantum efficiency (EQE) and low efficiency roll-off.[10,11] Generally, a considerable overlap of highest occupied molecular orbital (HOMO) and lowest unoccupied molecular orbital (LUMO) is conducive to a high oscillator strength (f) and then a high k_F.[12–14] However, for achieving a high k_{RISC}, the most effective strategy is to reduce the splitting energy between the lowest triplet state (T_1) and the lowest singlet state (S_1), *i.e.*, ΔE_{ST}, by decreasing the overlap of the HOMO and LUMO.[1,4,13] It follows that achieving high k_F and k_{RISC} simultaneously is of some difficulty in TADF materials, which is an obstacle for achieving high EQE and low efficiency roll-off simultaneously.

With regard to the TBCT-based TADF materials, appropriate donors/acceptors that possess suitable electron donating/accepting abilities are generally combined through a conjugated unit, and the torsion angels between the donors and acceptors should be subtly manipulated to give suitable HOMO–LUMO overlaps and thus high k_F.[2,4,15–17] As for the TSCT-based TADF materials, the CT process occurs through the spatial π–π interaction of the donors and acceptors. The tiny overlaps of the HOMOs and LUMOs for this kind of material generally give high k_{RISC}.[18–21] It appears that concurrent intramolecular TBCT and TSCT might be an effective way to achieve high k_F and k_{RISC} simultaneously. Unfortunately, the majority of the reported intramolecular TSCT-based materials mainly emphasized the

State Key Laboratory of Luminescent Materials and Devices, Institute of Polymer Optoelectronic Materials and Devices, South China University of Technology, Wushan Road 381, Guangzhou 510640, P. R. China. E-mail: mssjsu@scut.edu.cn

† Electronic supplementary information (ESI) available. See DOI: https://doi.org/10.1039/d2qm01363k

existence of TSCT without too much consideration of TBCT.[20–22] Although a few research studies have paid attention to the coexistence of intramolecular TBCT and TSCT,[5,14,23,24] systematic manipulation of the intramolecular TBCT and TSCT was not mentioned.

Due to the strong CT characteristic, D–A-type TADF emitters, including TBCT and TSCT type molecules, exhibit a broad electroluminescence (EL) band with a typical full-width at half-maximum (FWHM) of 80–100 nm. To address this crucial flaw, Hatakeyama *et al.*[25,26] reported a new design strategy featuring an alternating HOMO/LUMO pattern, based on the multiple resonance (MR) effect of boron and nitrogen/oxygen atoms. Most MR-based molecules possess a narrow emission band owing to the suppressed vibronic coupling between the ground (S_0) and singlet excited (S_1) states. Even though these MR-TADF emitters rendered excellent performance in OLED devices, severe efficiency roll-off at high current density can be observed due to their relatively large ΔE_{ST}.[25,27–30] To overcome this drawback, great efforts have been made in molecular design and device design, such as increasing k_{RISC} and using a phosphor or TADF molecule as an assistant host (sensitizer) to improve the device performance and reduce the efficiency roll-off of the devices with MR-TADF materials as terminal emitters.[5,31–37]

In this research, three TADF molecules, *o*-Cz-TRZ, *o*-DCz-TRZ and *o*-TCz-TRZ, are constructed by an oligo carbazole donor and diphenyltriazine acceptor *ortho*-connected to a benzene linker (Fig. 1). The *ortho*-linkage between the donor and acceptor is conducive to inducing intramolecular TSCT characteristics for the short spatial distance of the donor and acceptor while retaining TBCT characteristics through the HOMO–LUMO overlap localized at the benzene linker. The proportions of intramolecular TBCT and TSCT are easily modulated by the number of carbazole units. Benefitting from the concurrent intramolecular TBCT and TSCT, k_F exceeding 10^6 s^{-1} and k_{RISC} approaching 10^6 s^{-1} are achieved simultaneously for all the developed materials. *o*-DCz-TRZ with 70.0% intramolecular TSCT characteristic and 25.5% TBCT characteristic gives the highest k_{RISC} and photoluminescence quantum yield (PLQY) and a relatively high k_F among the three compounds, resulting in a maximum EQE of 20.3% and a low efficiency roll-off of 11.8% at 1000 cd m^{-2} for the device based on *o*-DCz-TRZ as the emitter. Furthermore, by using these materials as assistant hosts and sensitizers and DMAc-BN as a terminal emitter,[29,30] high efficiencies of 23.9% and 66.0 lm W^{-1} are achieved for the device sensitized by *o*-TCz-TRZ, featuring a FWHM of 46 nm and a slow efficiency roll-off with EQE of 17.9% at the luminance of 1000 cd m^{-2}. The current work provides a simple molecular design strategy of tunable intramolecular TBCT and TSCT for TADF molecules with simultaneous high k_F and k_{RISC} toward high-efficiency and low efficiency roll-off OLEDs.

Results and discussion

Synthesis and characterization

The molecular structures and synthetic routes are illustrated in Fig. 1 and Scheme S1 (ESI†). The intermediate 2-(2-fluorophenyl)-4,6-diphenyl-1,3,5-triazine and target product *o*-Cz-TRZ were synthesized according to the reported literature.[38,39] The chemical structures of all the materials were determined by ^{1}H NMR, ^{13}C NMR and mass spectra. Thermogravimetric analysis (Fig. S1a, ESI†) reveals that all the compounds exhibit good thermal stability with high decomposition temperatures (T_d, corresponding to a weight loss of 5 wt%) over 360 °C (Table S1, ESI†). According to the differential scanning calorimetry (DSC) analysis, all the compounds exhibit obvious glass transition processes with glass transition temperatures (T_g) of 62, 120 and 165 °C for *o*-Cz-TRZ, *o*-DCz-TRZ and *o*-TCz-TRZ, respectively. No obvious melting processes were observed for *o*-DCz-TRZ and *o*-TCz-TRZ in the range of 0–300 °C whereas *o*-Cz-TRZ exhibits a melting point (T_m) of 210 °C. In addition, distinct

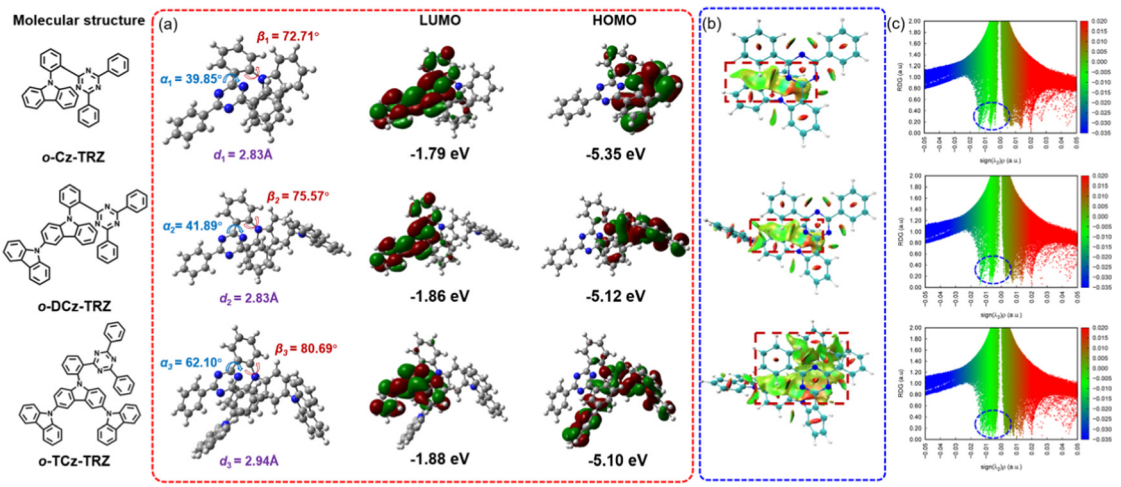

Fig. 1 Chemical structures and optimized molecular geometries of the ground states and FMO distributions and energy levels (a) simulated at the B3LYP/6-31G** level. RDG isosurfaces (b) and RDG scattering diagrams (c) based on DFT simulations for *o*-Cz-TRZ, *o*-DCz-TRZ and *o*-TCz-TRZ, respectively.

non-equilibrium crystal transformation processes were observed for all the compounds (Fig. S1b, ESI†). Electrochemical properties were investigated by cyclic voltammetry (CV) measurements (Fig. S2, ESI†), and the HOMO energy levels were estimated to be −5.52, −5.38 and −5.37 eV for *o*-Cz-TRZ, *o*-DCz-TRZ and *o*-TCz-TRZ, respectively, from the onset potentials of the redox peaks according to Eqn S1 (Table S1, ESI†).

Computational simulations

To gain insight into the molecular structures and electron distributions, density functional theory (DFT) and time-dependent DFT (TD-DFT) simulations were conducted based on the B3LYP/6-31G** level. As depicted in Fig. 1 in the ground state geometry, the *ortho*-connected donor and acceptor lead to approximately face-to-face alignment of the oligo carbazole and triazine rings on the phenylene bridge, which ensures the occurrence of intramolecular TSCT from the donor to the acceptor directly. Attributed to the *ortho*-linkage and the large steric hindrance, these molecules exhibit a twisted structure with torsion angles between the oligo carbazole donor and benzene linker (β, red curved arrow) of 72.71°, 75.57°, and 80.69° for *o*-Cz-TRZ, *o*-DCz-TRZ and *o*-TCz-TRZ, respectively. Such large torsion angles are beneficial to separate the HOMOs and LUMOs, leading to small computational ΔE_{ST}s of 90, 50 and 30 meV for *o*-Cz-TRZ, *o*-DCz-TRZ and *o*-TCz-TRZ, respectively (Fig. 1). With increasing number of carbazole units, both the torsion angles of α (the torsion angle between the benzene linker and diphenyltriazine acceptor) and β increase in varying degrees. Furthermore, the HOMO–LUMO overlap at the benzene linker is reduced, leading to low oscillator strength (f = 0.0052, 0.0040 and 0.0022 for *o*-Cz-TRZ, *o*-DCz-TRZ and *o*-TCz-TRZ, respectively, as shown in Fig. S3, ESI†).

In order to investigate the intramolecular weak interactions of these materials, reduced density gradient (RDG) isosurfaces and scattering diagrams were performed in virtue of Multiwfn and visual molecular dynamics (VMD) (Fig. 1).[40–42] As illustrated in Fig. 1b, a noticeable non-covalent weak interaction between the oligo carbazole donor and diphenyltriazine acceptor can be observed in the RDG isosurfaces (the green area in the red dotted box), which demonstrates the existence of intramolecular TSCT intuitively.[5,7,19,21] The non-covalent weak interactions are strengthened with increasing number of carbazole units, which can be embodied in the larger areas in the RDG isosurfaces. Besides, the more intensive spikes are observed as shown in the RDG scattering diagrams (Fig. 1c, the green spikes in the blue dotted circles), demonstrating the effectiveness of intramolecular TSCT modulation by the structure of the donor. Moreover, the interfragment charge transfer (IFCT) analysis based on the TD-DFT calculation results was conducted, which quantitatively depicted the contribution of electron transfer among the fragments (donor, acceptor and linker).[5,19,21] The interaction ratios of TSCT in the S_1 state were calculated to be 0.6376, 0.7002 and 0.924 for *o*-Cz-TRZ, *o*-DCz-TRZ and *o*-TCz-TRZ, respectively, according to the reported literature.[5]

Photophysical properties

Ultraviolet-visible (UV-vis) absorption and photoluminescence (PL) spectra of these molecules were measured in diluted toluene solution (Fig. 2a). For all the target molecules, the relatively strong absorption bands at around 310–350 nm mainly originate from the local excited (LE) state transition of the carbazole-based donors, and the tail absorption bands at around 350–440 nm could be attributed to the intramolecular charge-transfer (ICT) transition (Fig. 3a). The optical bandgaps (E_gs) are estimated to be 2.63, 2.52 and 2.52 eV for *o*-Cz-TRZ, *o*-DCz-TRZ and *o*-TCz-TRZ, respectively, from the onset of the absorption spectra. In the PL spectra, *o*-Cz-TRZ exhibits a blue emission peak at 460 nm while *o*-DCz-TRZ and *o*-TCz-TRZ exhibit sky-blue emission peaks at 495 and 492 nm, respectively. In comparison with *o*-Cz-TRZ, the bathochromic shift of the PL spectra for *o*-DCz-TRZ and *o*-TCz-TRZ should be attributed to the stronger electron-donating ability of the DCz and TCz donor units, which is consistent with the tendency of HOMO energy levels attained from the CV measurements. Nearly superimposed low-temperature fluorescence and phosphorescence spectra were observed in toluene solution (Fig. S5, ESI†), resulting in tiny ΔE_{ST}s approaching zero for all the materials (Table 1), which are consistent with the TD-DFT calculations. In accordance with the natural transition orbital (NTO) analysis of the S_1 and T_1 states (Fig. S3, ESI†), the broad

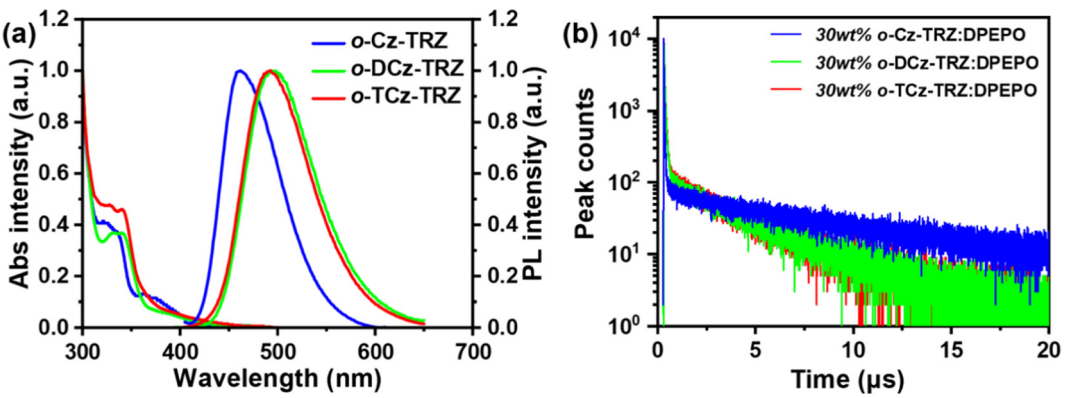

Fig. 2 (a) UV-vis absorption and PL spectra of *o*-Cz-TRZ, *o*-DCz-TRZ and *o*-TCz-TRZ in diluted toluene solution. (b) Transient PL decay curves of *o*-Cz-TRZ, *o*-DCz-TRZ and *o*-TCz-TRZ doped in DPEPO films (30 wt%).

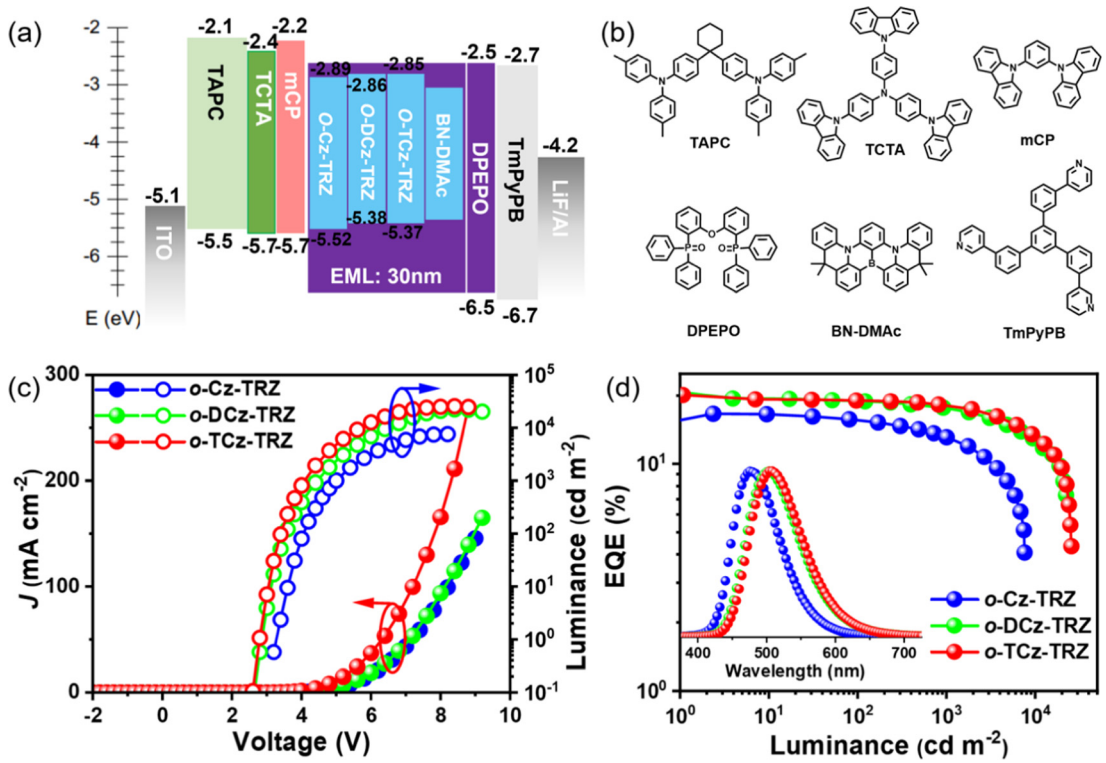

Fig. 3 (a) Device architecture and its energy level diagram. (b) Chemical structures of the corresponding materials. (c) Current density–Voltage–Luminance (*J*–*V*–*L*) curves, (d) EQE-luminance curves and EL spectra (inset) of the devices based on *o*-Cz-TRZ, *o*-DCz-TRZ and *o*-TCz-TRZ as the emitter.

Table 1 Photophysical properties of the investigated molecules doped into DPEPO films at the concentration of 30 wt% at room temperature

Compound	λ_{em} (nm)	PLQY (%)	ϕ_{PF} (%)	ϕ_{DF} (%)	ϕ_{ISC} (%)	τ_{PF} (ns)	τ_{DF}[a] (μs)	k_F (10^6 s^{-1})	k_{IC} (10^6 s^{-1})	k_{ISC} (10^7 s^{-1})	k_{RISC} (10^5 s^{-1})	k_F/k_{IC}	k_{RISC}/k_{ISC} (10^{-2})
o-Cz-TRZ	475	65.7	26.3	39.4	73.7	26.7	8.2	9.8	5.1	2.8	2.5	1.9	0.9
o-DCz-TRZ	495	82.5	24.3	51.5	75.7	58.9	3.8	4.1	1.3	1.3	7.3	3.2	5.6
o-TCz-TRZ	498	80.6	15.9	36.4	84.1	52.3	3.9	3.0	2.8	1.6	7.0	1.1	4.4

[a] Average lifetime calculated by $\tau_{av} = \sum_i^A \tau_i^2 \Big/ \sum_i^A \tau_i$, where A_i is the pre-exponential for lifetime τ_i.

and featureless fluorescence and phosphorescence spectra confirm the CT characteristics of the singlet and triplet states. Significant positive solvatochromism effects were observed as the embodiment of the strong CT characteristics for all the materials (Fig. S6, ESI†).

The solid-state photophysical properties of all the compounds were investigated by doping them into a typical host material bis[2-(diphenylphosphino)phenyl] ether oxide (DPEPO)[43] in a concentration of 30 wt%. All these doped films exhibit the typical emissions from *o*-Cz-TRZ, *o*-DCz-TRZ and *o*-TCz-TRZ with emission peaks of 475, 495 and 498 nm, respectively (Fig. S8, ESI†). The energy levels of the S_1/T_1 states in the 30 wt% doped films were estimated to be 2.92/2.85, 2.87/2.83 and 2.85/2.82 eV from the onset of the low-temperature fluorescence and phosphorescence spectra (Fig. S7, ESI†), resulting in tiny ΔE_{ST}s of 70, 40 and 30 meV for *o*-Cz-TRZ, *o*-DCz-TRZ and *o*-TCz-TRZ, respectively, which are conducive to the RISC process and TADF emission.

To verify the TADF characteristics, transient PL decay curves were measured in the doped films and are provided in Fig. 2b and Fig. S7 (ESI†). All these materials exhibit double-exponential decays with prompt lifetime (τ_{PF}) of 26–59 ns and delayed lifetime (τ_{DF}) of 3.8–8.2 μs, demonstrating their TADF characteristics, which is in agreement with the tiny experimental ΔE_{ST}s. Furthermore, from the temperature-dependent transient PL decay curves, the enhancement of the delayed fluorescence ratio with increased temperature from 100 K to 300 K further confirms the TADF characteristics (Fig. S7, ESI†).[1,3] The PLQYs of the *o*-Cz-TRZ, *o*-DCz-TRZ and *o*-TCz-TRZ doped films were measured to be 65.7%, 82.5% and 80.6%, respectively. Based on the transient PL decay spectra in the microsecond scale and PLQYs, high k_F of 2.0–9.8 × 10^6 s^{-1} and k_{RISC} of 2.5–7.3 × 10^5 s^{-1} were simultaneously achieved for these molecules (Table 1). As expected, k_F and k_{RISC} could be modulated by simply changing the number of carbazole units, which confirms the effectiveness of the molecular

design strategy, *i.e.*, modulating the PL properties and the exciton dynamic processes through adjusting the balance between intramolecular TBCT and TSCT. With increasing number of carbazole units, the k_F diminishes gradually mainly due to the gradually reduced overlap of the HOMOs and LUMOs. It follows that both intramolecular TBCT and TSCT contribute to promoting k_F but TBCT through the benzene linker (overlap of HOMOs and LUMOs locate at the linker) plays a more significant role than TSCT. Combining k_F and k_{IC} and comparing their ratios, that is, k_F/k_{IC} are 1.9, 3.2 and 1.1 for *o*-Cz-TRZ, *o*-DCz-TRZ and *o*-TCz-TRZ, respectively, the variation of PLQY (65.7%, 77.9% and 52.3% for *o*-Cz-TRZ, *o*-DCz-TRZ and *o*-TCz-TRZ, respectively) could be explained, which demonstrates the effectiveness of modulating k_F and PLQY by simply manipulating the proportion between intramolecular TBCT and TSCT. The k_{RISC}s of *o*-DCz-TRZ (7.3×10^5 s^{-1}) and *o*-TCz-TRZ (7.0×10^5 s^{-1}) are higher than that of *o*-Cz-TRZ (2.5×10^5 s^{-1}), which can mainly be attributed to the stronger non-covalent interactions contributing to the strengthened SOC and the lower ΔE_{ST}. As shown in Table 1, the k_{RISC}/k_{ISC} values are 0.9, 5.6 and 4.4 ($\times 10^{-2}$) for *o*-Cz-TRZ, *o*-DCz-TRZ and *o*-TCz-TRZ, respectively, demonstrating that the RISC processes are effectively promoted by greater intramolecular TSCT characters, which contributes to a higher triplet exciton utilization. Furthermore, the higher triplet exciton utilization and the higher k_{RISC} are conducive to high EQE and reduced efficiency roll-off especially at a high current density for a device.

From the above results and analysis, it is not difficult to find that TBCT plays a more significant role in promoting k_F *via* the overlap of the HOMOs and LUMOs at the benzene linker while intramolecular TSCT tends to contribute more to modulating k_{RISC} through the non-covalent weak interactions. Besides, it is worth noting that k_{RISC} can be improved with a relatively higher proportion of intramolecular TSCT characteristic but excessive intramolecular TSCT components have no significant effects on further promotion of k_{RISC} mainly on account of the reduced TBCT components, which also contribute to the promoted k_{RISC}. Therefore, the balance between intramolecular TSCT and TBCT for achieving relatively balanced k_{RISC}, k_F and PLQY should be clarified and emphasized. An optimum balance could be found for *o*-DCz-TRZ, which possesses the highest PLQY and k_{RISC} and a relatively high k_F, making it a potential candidate to achieve high EQE and low efficiency roll-off in the corresponding device.

To evaluate the performances of those materials as assistant hosts, a green MR-TADF emitter BN-DMAc with an emission peak at 484 nm, a small FWHM of 29 nm and a high PLQY of 88% was used as the terminal emitter.[29,30] Significant absorption–emission spectral overlap was found between BN-DMAc and the assistant hosts (Fig. S10, ESI†), indicating the efficient energy transfer from the assistant hosts to BN-DMAc. The emission spectra of the ternary doped films DPEPO: 30 wt% sensitizers: 1 wt% BN-DMAc were measured and illustrated in Fig. S11 (ESI†). In all cases, the emission from the assistant hosts is almost eliminated with a peak at 494 nm and slightly broadened FWHMs of 40–43 nm, indicating the efficient energy transfer from the assistant hosts to BN-DMAc. The slightly broadened FWHMs of these films can be attributed to the high polarity of DPEPO and these assistant hosts. In addition, τ_{DF}s of 19.8–21.9 μs were detected while using these molecules as the assistant host. Compared with BN-DMAc doped in the conventional DPEPO host, increased proportions of the delayed components were realized (Fig. S11 and Table S2, ESI†), indicating that the device performance of BN-DMAc can be improved by the assistant hosts under these conditions.

OLED performance

To verify the application potential of these compounds and understand the relationship between the electroluminescence (EL) performances and the molecular structures, OLED devices were fabricated with a device architecture of ITO/TAPC (30 nm)/TCTA (10 nm)/mCP (10 nm)/DPEPO: 30 wt% emitters (30 nm)/DPEPO (10 nm)/TmPyPB (40 nm)/LiF (1 nm)/Al (150 nm), where (1,1-bis(4-(*N*,*N*-di(p-tolyl)-amino)-phenyl)cyclohexane (TAPC), 4,4′,4″tris(*N*-carbazolyl)triphenylamine (TCTA), 1,3-bis(*N*-carbazolyl)benzene (mCP), DPEPO, 1,3,5-tri(m-pyrid-3-ylphenyl)benzene (TmPyPB) and LiF layers play the roles of hole injection and hole-transport, electron-blocking, hole-blocking, electron transport and electron injection layers, respectively, as illustrated in Fig. 3. The device characteristics are depicted in Fig. 3 and Fig. S12 (ESI†) and the EL parameters are summarized in Table S4 (ESI†).

The devices based on *o*-Cz-TRZs, *o*-DCz-TRZ and *o*-TCz-TRZ as the emitter exhibit sky-blue to green emissions with peaks of 477, 500 and 505 nm, and the corresponding Commission Internationale de l'Eclairage (CIE) color coordinates are (0.16, 0.27), (0.23, 0.46) and (0.24, 0.49), respectively (Fig. 3d and Table S3, ESI†). Noticeably, *o*-DCz-TRZ and *o*-TCz-TRZ exhibit higher efficiencies with maximum EQEs of 20.3% and 20.1%, maximum power efficiencies (PEs) of 64.9 and 64.8 lm W^{-1}, and maximum current efficiencies (CEs) of 57.8 and 57.8 cd A^{-1}, respectively, owing to their higher PLQYs. Furthermore, benefitting from the high k_{RISC}, low efficiency roll-offs of 11.8% and 9.9% were also observed for the devices based on *o*-DCz-TRZ and *o*-TCz-TRZ (Fig. 3 and Table S3, ESI†) at the practical luminance of 1000 cd m^{-2}, respectively. The simulated exciton annihilation processes of all the devices based on triplet–triplet annihilation (TTA) and singlet-polaron annihilation (SPA) models agree well with the experimental results, as shown in Fig. S13 (ESI†),[44–46] which demonstrates that TTA is the dominant mechanism for exciton annihilation at low current density and SPA can account for the efficiency roll-off at high current density in these devices.

The devices using these materials as the assistant host and BN-DMAc as the terminal emitter were fabricated in a structure of ITO/TAPC (30 nm)/TCTA (10 nm)/mCP (10 nm)/DPEPO: 30 wt% sensitizers: 1 wt% BN-DMAc (30 nm)/DPEPO (10 nm)/TmPyPB (40 nm)/LiF (1 nm)/Al (150 nm). In the ternary doped emission layer, the concentration of the terminal emitter BN-DMAc was optimized to 1 wt% to reduce the Dexter energy transfer process from the hosts. For comparison, the device without an assistant host was also fabricated. The devices with assistant hosts exhibit significantly suppressed efficiency roll-off and improved device performance owing to the high k_r of

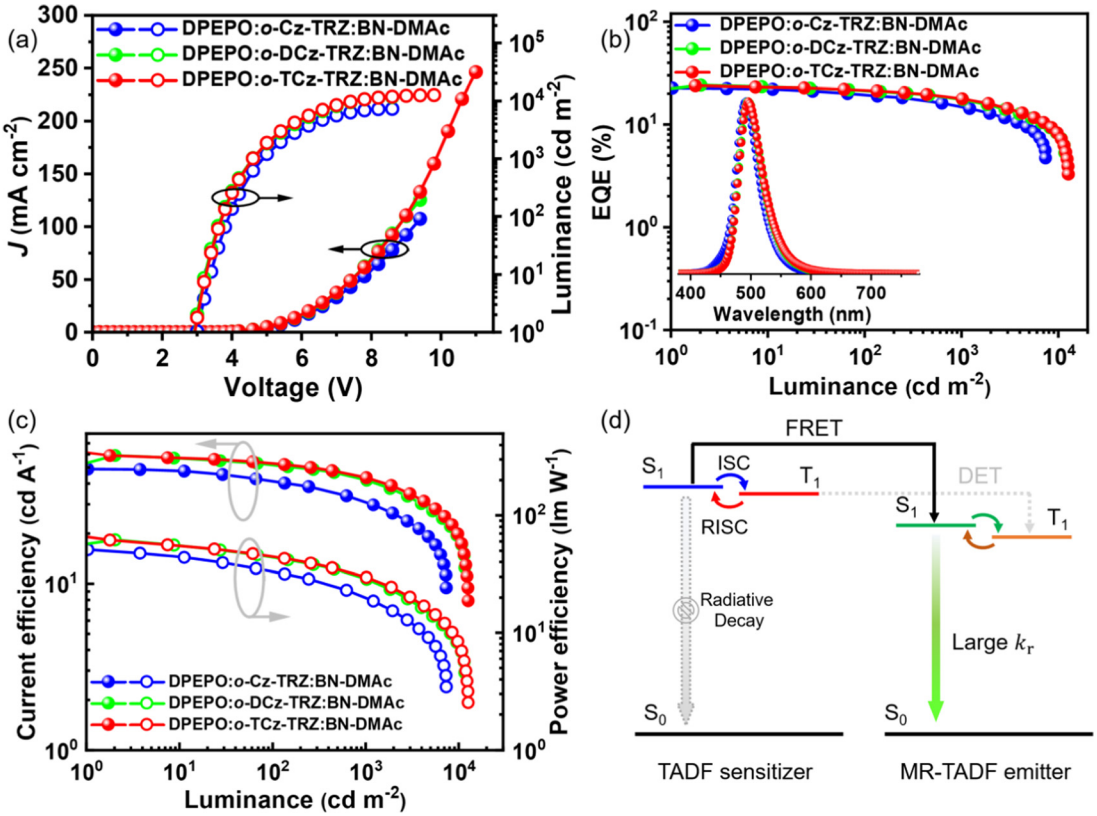

Fig. 4 *J*–*V*–*L* curves (a), efficiency curves (b and c) and energy transfer mechanism (d) of the devices using *o*-Cz-TRZ, *o*-DCz-TRZ and *o*-TCz-TRZ as assistant hosts.

BN-DMAc and high k_{RISC} of the sensitizers. The Förster energy transfer (FRET) from the assistant host to the dopant can be quantified by utilizing the rate of FRET (k_{ET}), the efficiency of FRET ($\varnothing_{ET}$) and the FRET radius (R_0). The results show that *o*-Cz-TRZ exhibits small R_0 and lower k_{ET} and $\varnothing_{ET}$ than those of *o*-DCz-TRZ and *o*-TCz-TRZ (Table S4, ESI†), evidencing the more efficient energy transfer from *o*-DCz-TRZ and *o*-TCz-TRZ to BN-DMAc. Fig. 4b depicts the EL spectra of the *o*-Cz-TRZ, *o*-DCz-TRZ and *o*-TCz-TRZ sensitized devices, exhibiting FWHMs of 44, 46 and 46 nm with identical emission peaks of 492, 496 and 496 nm and corresponding CIE coordinates of (0.12, 0.40), (0.13, 0.49) and (0.14, 0.49), respectively. The V_{on}s of these devices are 2.9–3.0 V (Fig. 4a), indicating efficient carrier injection and transport characteristics. Similarly, the devices using *o*-DCz-TRZ and *o*-TCz-TRZ as assistant hosts achieve better performance, with maximum EQEs of 24.2% and 23.9%, CEs of 59.1 and 61.7 cd A^{-1} and PEs of 61.9 and 66.0 lm W^{-1} (Fig. 4 and Table S5, ESI†), respectively, which are higher than those of the devices with the same terminal emitter BN-DMAc using mCBP or DPEPO hosts (Fig. S14 and Table S5, ESI†) and comparable to the device using mCBP and PO-T2T exciplex hosts (Table S6, ESI†). What's more, compared with the DPEPO hosted device (Fig. S14 and Table S5, ESI†), these devices achieve higher efficiency and luminance and reduced efficiency roll-off. For example, the *o*-TCz-TRZ sensitized device exhibits EQEs of 21.5% and 17.9% at the practical luminance of 100 and 1000 cd m^{-2}, respectively, corresponding to efficiency reduction of 10.0% and 16.9% relative to the maximum EQE, which are also better than the devices using typical mCBP and exciplex hosts (mCBP:PO-T2T).[29,30] After the introduction of assistant hosts, the predominant energy transfer pathway is changed to the long-range FRET from the assistant host to BN-DNAc, the population of triplet excitons on BN-DMAc can be greatly reduced to improve the exciton utilization and reduce the corresponding quenching effect (Fig. 4d), resulting in high efficiency and reduced efficiency roll-off.

Conclusion

In summary, three TADF molecules are successfully designed and synthesized through the *ortho*-linkage of the diphenyltriazine acceptor and the oligo carbazole donor to the benzene linker. Combining the computational simulation and experimental analysis, the concurrent intramolecular TBCT and TSCT are confirmed and the ratios are successfully modulated by simply controlling the number of carbazole units. Through delicately balanced intramolecular TSCT and TBCT, relatively high k_F and k_{RISC} are achieved simultaneously. Benefitting from the high PLQY and k_{RISC}, the device using *o*-DCz-TRZ as an emitter gives maximum efficiencies of 20.3% and 64.9 lm W^{-1}, characterized by slow efficiency roll-off with EQE of 17.9% at

the luminance of 1000 cd m^{-2}. Furthermore, by using these materials as assistant hosts and sensitizers and DMAc-BN as a terminal emitter, high efficiencies of 23.9% and 66.0 lm W^{-1} are achieved with FWHM of 46 nm, featuring slow efficiency roll-off with EQE of 17.9% at the luminance of 1000 cd m^{-2}. This reveals the importance of modulating the balance of intramolecular TBCT and TSCT in TADF materials towards high k_F and k_{RISC} rates and thus high efficiency and low efficiency roll-off OLEDs.

Conflicts of interest

There are no conflicts to declare.

Acknowledgements

The authors greatly appreciate the financial support from the National Key R&D Program of China (2020YFA0714600), the National Natural Science Foundation of China (52273179, 91833304, 51625301, 52003088 and 51861145301), the Guangdong Provincial Department of Science and Technology (2019A1515012059), and the China Postdoctoral Science Foundation Funded Project (2021M701234).

References

1 H. Uoyama, K. Goushi, K. Shizu, H. Nomura and C. Adachi, Highly efficient organic light-emitting diodes from delayed fluorescence, *Nature*, 2012, **492**, 234–238.
2 Q. Zhang, J. Li, K. Shizu, S. Huang, S. Hirata, H. Miyazaki and C. Adachi, Design of efficient thermally activated delayed fluorescence materials for pure blue organic light emitting diodes, *J. Am. Chem. Soc.*, 2012, **134**, 14706–14709.
3 H. Tanaka, K. Shizu, H. Miyazaki and C. Adachi, Efficient green thermally activated delayed fluorescence (TADF) from a phenoxazine-triphenyltriazine (PXZ-TRZ) derivative, *Chem. Commun.*, 2012, **48**, 11392–11394.
4 L. S. Cui, H. Nomura, Y. Geng, J. U. Kim, H. Nakanotani and C. Adachi, Controlling Singlet-Triplet Energy Splitting for Deep-Blue Thermally Activated Delayed Fluorescence Emitters, *Angew. Chem., Int. Ed.*, 2017, **56**, 1571–1575.
5 T. Huang, Q. Wang, S. Xiao, D. Zhang, Y. Zhang, C. Yin, D. Yang, D. Ma, Z. Wang and L. Duan, Simultaneously Enhanced Reverse Intersystem Crossing and Radiative Decay in Thermally Activated Delayed Fluorophors with Multiple Through-space Charge Transfers, *Angew. Chem., Int. Ed.*, 2021, **60**, 23771–23776.
6 W. Li, B. Li, X. Cai, L. Gan, Z. Xu, W. Li, K. Liu, D. Chen and S. J. Su, Tri-Spiral Donor for High Efficiency and Versatile Blue Thermally Activated Delayed Fluorescence Materials, *Angew. Chem., Int. Ed.*, 2019, **58**, 11301–11305.
7 Z. Zhao, C. Zeng, X. Peng, Y. Liu, H. Zhao, L. Hua, S. J. Su, S. Yan and Z. Ren, Tuning Intramolecular Stacking of Rigid Heteroaromatic Compounds for High-Efficiency Deep-Blue Through-Space Charge-Transfer Emission, *Angew. Chem., Int. Ed.*, 2022, **61**, e202210864.
8 C. Duan, Y. Xin, Z. Wang, J. Zhang, C. Han and H. Xu, High-efficiency hyperfluorescent white light-emitting diodes based on high-concentration-doped TADF sensitizer matrices via spatial and energy gap effects, *Chem. Sci.*, 2021, **13**, 159–169.
9 F. Gao, R. Du, C. Han, J. Zhang, Y. Wei, G. Lu and H. Xu, High-efficiency blue thermally activated delayed fluorescence from donor-acceptor-donor systems via the through-space conjugation effect, *Chem. Sci.*, 2019, **10**, 5556–5567.
10 L. Gan, Z. D. Xu, Z. H. Wang, B. B. Li, W. Li, X. Y. Cai, K. K. Liu, Q. M. Liang and S. J. Su, Utilizing a Spiro TADF Moiety as a Functional Electron Donor in TADF Molecular Design toward Efficient Multichannel Reverse Intersystem Crossing, *Adv. Funct. Mater.*, 2019, **29**, 1808088.
11 X. Cai, X. Li, G. Xie, Z. He, K. Gao, K. Liu, D. Chen, Y. Cao and S. J. Su, Rate-limited effect of reverse intersystem crossing process: the key for tuning thermally activated delayed fluorescence lifetime and efficiency roll-off of organic light emitting diodes, *Chem. Sci.*, 2016, **7**, 4264–4275.
12 X. K. Chen, D. Kim and J. L. Bredas, Thermally Activated Delayed Fluorescence (TADF) Path toward Efficient Electroluminescence in Purely Organic Materials: Molecular Level Insight, *Acc. Chem. Res.*, 2018, **51**, 2215–2224.
13 P. Rajamalli, N. Senthilkumar, P. Gandeepan, P. Y. Huang, M. J. Huang, C. Z. Ren-Wu, C. Y. Yang, M. J. Chiu, L. K. Chu, H. W. Lin and C. H. Cheng, A New Molecular Design Based on Thermally Activated Delayed Fluorescence for Highly Efficient Organic Light Emitting Diodes, *J. Am. Chem. Soc.*, 2016, **138**, 628–634.
14 X. K. Chen, B. W. Bakr, M. Auffray, Y. Tsuchiya, C. D. Sherrill, C. Adachi and J. L. Bredas, Intramolecular Noncovalent Interactions Facilitate Thermally Activated Delayed Fluorescence (TADF), *J. Phys. Chem. Lett.*, 2019, **10**, 3260–3268.
15 J. U. Kim, I. S. Park, C. Y. Chan, M. Tanaka, Y. Tsuchiya, H. Nakanotani and C. Adachi, Nanosecond-time-scale delayed fluorescence molecule for deep-blue OLEDs with small efficiency rolloff, *Nat. Commun.*, 2020, **11**, 1765.
16 T.-L. Wu, M.-J. Huang, C.-C. Lin, P.-Y. Huang, T.-Y. Chou, R.-W. Chen-Cheng, H.-W. Lin, R.-S. Liu and C.-H. Cheng, Diboron compound-based organic light-emitting diodes with high efficiency and reduced efficiency roll-off, *Nat. Photonics*, 2018, **12**, 235–240.
17 J. Zhang, D. Ding, Y. Wei, F. Han, H. Xu and W. Huang, Multiphosphine-Oxide Hosts for Ultralow-Voltage-Driven True-Blue Thermally Activated Delayed Fluorescence Diodes with External Quantum Efficiency beyond 20, *Adv. Mater.*, 2016, **28**, 479–485.
18 H. Tsujimoto, D. G. Ha, G. Markopoulos, H. S. Chae, M. A. Baldo and T. M. Swager, Thermally Activated Delayed Fluorescence and Aggregation Induced Emission with Through-Space Charge Transfer, *J. Am. Chem. Soc.*, 2017, **139**, 4894–4900.

19 X. Tang, L. S. Cui, H. C. Li, A. J. Gillett, F. Auras, Y. K. Qu, C. Zhong, S. T. E. Jones, Z. Q. Jiang, R. H. Friend and L. S. Liao, Highly efficient luminescence from space-confined charge-transfer emitters, *Nat. Mater.*, 2020, **19**, 1332–1338.
20 Y. Wada, H. Nakagawa, S. Matsumoto, Y. Wakisaka and H. Kaji, Organic light emitters exhibiting very fast reverse intersystem crossing, *Nat. Photonics*, 2020, **14**, 643–649.
21 F. Ni, C. W. Huang, Y. Tang, Z. Chen, Y. Wu, S. Xia, X. Cao, J. H. Hsu, W. K. Lee, K. Zheng, Z. Huang, C. C. Wu and C. Yang, Integrating molecular rigidity and chirality into thermally activated delayed fluorescence emitters for highly efficient sky-blue and orange circularly polarized electroluminescence, *Mater. Horiz.*, 2021, **8**, 547–555.
22 K. Li, Y. Zhu, B. Yao, Y. Chen, H. Deng, Q. Zhang, H. Zhan, Z. Xie and Y. Cheng, Rotation-restricted thermally activated delayed fluorescence compounds for efficient solution-processed OLEDs with EQEs of up to 24.3% and small roll-off, *Chem. Commun.*, 2020, **56**, 5957–5960.
23 X. Lv, Y. Wang, N. Li, X. Cao, G. Xie, H. Huang, C. Zhong, L. Wang and C. Yang, Regulating the photophysical properties of highly twisted TADF emitters by concurrent through-space/-bond charge transfer, *Chem. Eng. J.*, 2020, **402**, 126173.
24 H. Miranda-Salinas, Y.-T. Hung, Y.-S. Chen, D. Luo, H.-C. Kao, C.-H. Chang, K.-T. Wong and A. Monkman, Controlling through-space and through-bond intramolecular charge transfer in bridged D–D′–A TADF emitters, *J. Mater. Chem. C*, 2021, **9**, 8819–8833.
25 T. Hatakeyama, K. Shiren, K. Nakajima, S. Nomura, S. Nakatsuka, K. Kinoshita, J. Ni, Y. Ono and T. Ikuta, Ultrapure Blue Thermally Activated Delayed Fluorescence Molecules: Efficient HOMO-LUMO Separation by the Multiple Resonance Effect, *Adv. Mater.*, 2016, **28**, 2777–2781.
26 Y. Kondo, K. Yoshiura, S. Kitera, H. Nishi, S. Oda, H. Gotoh, Y. Sasada, M. Yanai and T. Hatakeyama, Narrowband deep-blue organic light-emitting diode featuring an organoboron-based emitter, *Nat. Photonics*, 2019, **13**, 678–682.
27 Y. C. Xu, Z. Cheng, Z. Q. Li, B. Y. Liang, J. X. Wang, J. B. Wei, Z. L. Zhang and Y. Wang, Molecular-Structure and Device-Configuration Optimizations toward Highly Efficient Green Electroluminescence with Narrowband Emission and High Color Purity, *Adv. Opt. Mater.*, 2020, **8**, 1902142.
28 J. Bian, S. Chen, L. Qiu, R. Tian, Y. Man, Y. Wang, S. Chen, J. Zhang, C. Duan, C. Han and H. Xu, Ambipolar Self-Host Functionalization Accelerates Blue Multi-Resonance Thermally Activated Delayed Fluorescence with Internal Quantum Efficiency of 100, *Adv. Mater.*, 2022, **34**, e2110547.
29 P. Jiang, L. Zhan, X. Cao, X. Lv, S. Gong, Z. Chen, C. Zhou, Z. Huang, F. Ni, Y. Zou and C. Yang, Simple Acridan-Based Multi-Resonance Structures Enable Highly Efficient Narrowband Green TADF Electroluminescence, *Adv. Opt. Mater.*, 2021, **9**, 2100825.
30 G. T. Liu, H. Sasabe, K. Kumada, A. Matsunaga, H. Katagiri and J. Kido, Facile synthesis of multi-resonance ultra-pure-green TADF emitters based on bridged diarylamine derivatives for efficient OLEDs with narrow emission, *J. Mater. Chem. C*, 2021, **9**, 8308–8313.
31 Y. Zhang, D. Zhang, J. Wei, Z. Liu, Y. Lu and L. Duan, Multi-Resonance Induced Thermally Activated Delayed Fluorophores for Narrowband Green OLEDs, *Angew. Chem., Int. Ed.*, 2019, **58**, 16912–16917.
32 S. Y. Yang, Z. Q. Feng, Z. Y. Fu, K. Zhang, S. Chen, Y. J. Yu, B. Zou, K. Wang, L. S. Liao and Z. Q. Jiang, Highly Efficient Sky-Blue pi-Stacked Thermally Activated Delayed Fluorescence Emitter with Multi-Stimulus Response Properties, *Angew. Chem., Int. Ed.*, 2022, **61**, e202206861.
33 Y. Y. Qin, X. L. Yang, J. B. Jin, D. L. Li, X. W. Zhou, Z. Zheng, Y. J. Sun, W. Y. Wong, Y. Chi and S. J. Su, Facially Coordinated, Tris-bidentate Purin-8-ylidene Ir(III) Complexes for Blue Electrophosphorescence and Hyperluminescence, *Adv. Opt. Mater.*, 2022, **10**, 2201633.
34 C.-Y. Chan, M. Tanaka, Y.-T. Lee, Y.-W. Wong, H. Nakanotani, T. Hatakeyama and C. Adachi, Stable pure-blue hyperfluorescence organic light-emitting diodes with high-efficiency and narrow emission, *Nat. Photonics*, 2021, **15**, 203–207.
35 S. O. Jeon, K. H. Lee, J. S. Kim, S.-G. Ihn, Y. S. Chung, J. W. Kim, H. Lee, S. Kim, H. Choi and J. Y. Lee, High-efficiency, long-lifetime deep-blue organic light-emitting diodes, *Nat. Photonics*, 2021, **15**, 208–215.
36 H. Nakanotani, T. Higuchi, T. Furukawa, K. Masui, K. Morimoto, M. Numata, H. Tanaka, Y. Sagara, T. Yasuda and C. Adachi, High-efficiency organic light-emitting diodes with fluorescent emitters, *Nat. Commun.*, 2014, **5**, 4016.
37 D. Zhang, L. Duan, C. Li, Y. Li, H. Li, D. Zhang and Y. Qiu, High-Efficiency Fluorescent Organic Light-Emitting Devices Using Sensitizing Hosts with a Small Singlet–Triplet Exchange Energy, *Adv. Mater.*, 2014, **26**, 5050–5055.
38 D. Liu, D. Li, H. Meng, Y. Wang and L. Wu, Multifunctional applications of triazine/carbazole hybrid thermally activated delayed fluorescence emitters in organic light emitting diodes, *J. Mater. Chem. C*, 2019, **7**, 12470–12481.
39 J.-R. Cha, C. W. Lee, J. Y. Lee and M.-S. Gong, Design of ortho-linkage carbazole-triazine structure for high-efficiency blue thermally activated delayed fluorescent emitters, *Dyes Pigm.*, 2016, **134**, 562–568.
40 W. Humphrey, A. Dalke and K. Schulten, VMD: visual molecular dynamics, *J. Mol. Graphics*, 1996, **14**, 33–38.
41 E. R. Johnson, S. Keinan, P. Mori-Sanchez, J. Contreras-Garcia, A. J. Cohen and W. Yang, Revealing noncovalent interactions, *J. Am. Chem. Soc.*, 2010, **132**, 6498–6506.
42 T. Lu and F. Chen, Multiwfn: a multifunctional wavefunction analyzer, *J. Comput. Chem.*, 2012, **33**, 580–592.
43 C. Han, Y. Zhao, H. Xu, J. Chen, Z. Deng, D. Ma, Q. Li and P. Yan, A simple phosphine-oxide host with a multi-insulating structure: high triplet energy level for efficient blue electrophosphorescence, *Chem. – Eur. J.*, 2011, **17**, 5800–5803.
44 C. Murawski, K. Leo and M. C. Gather, Efficiency roll-off in organic light-emitting diodes, *Adv. Mater.*, 2013, **25**, 6801–6827.

45 H. Kuwae, A. Nitta, K. Yoshida, T. Kasahara, T. Matsushima, M. Inoue, S. Shoji, J. Mizuno and C. Adachi, Suppression of roll-off characteristics of organic light-emitting diodes by narrowing current injection/transport area to 50 nm, *Appl. Phys. Lett.*, 2015, **105**, 093301.

46 H. Kuwae, A. Nitta, K. Yoshida, T. Kasahara, T. Matsushima, M. Inoue, S. Shoji, J. Mizuno and C. Adachi, Suppression of external quantum efficiency roll-off of nanopatterned organic-light emitting diodes at high current densities, *J. Appl. Phys.*, 2015, **118**, 155501.

